

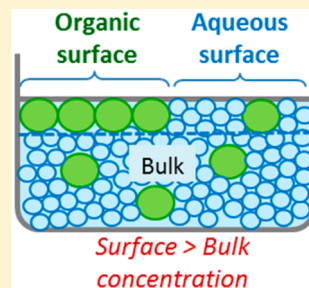
Phase Segregation at the Liquid–Air Interface Prior to Liquid–Liquid Equilibrium

Carolina Bermúdez-Salguero and Jesús Gracia-Fadrique*

Departamento de Fisicoquímica, Facultad de Química, Universidad Nacional Autónoma de México, Ciudad Universitaria, México, D.F. 04510, México

 Supporting Information

ABSTRACT: Binary systems with partial miscibility segregate into two liquid phases when their overall composition lies within the interval defined by the saturation points; out of this interval, there is one single phase, either solvent-rich or solute-rich. In most systems, in the one-phase regions, surface tension decreases with increasing solute concentration due to solute adsorption at the liquid–air interface. Therefore, the solute concentration at the surface is higher than in the bulk, leading to the hypothesis that phase segregation starts at the liquid–air interface with the formation of two surface phases, before the liquid–liquid equilibrium. This phenomenon is called surface segregation and is a step toward understanding liquid segregation at a molecular level and detailing the constitution of fluid interfaces. Surface segregation of aqueous binary systems of alkyl acetates with partial miscibility was theoretically demonstrated by means of a thermodynamic stability test based on energy minimization. Experimentally, the coexistence of two surface regions was verified through Brewster's angle microscopy. The observations were further interpreted with the aid of molecular dynamics simulations, which show the diffusion of the acetates from the bulk toward the liquid–air interface, where acetates aggregate into acetate-rich domains.



1. INTRODUCTION

Fluid phase equilibria are macroscopic phenomena which have been the subject of uncountable studies and of the development of a variety of experimental techniques to accurately measure temperature, pressure, and composition. Transition from one phase to another consists of the transfer of matter through the interface that separates them. Interface phenomena manifest themselves as the macroscopic surface tension, but the *in situ* study of interfaces requires microscopic and spectroscopic techniques to elucidate their structure and composition. The more detailed the understanding of the interface constitution, the more accurate will be the design of processes in which surface properties determine mass and momentum transfer, as in microfluidic devices,^{1,2} exfoliating media,^{3,4} or driven molecular assembly.^{5,6} In this work, the constitution of the liquid–air interface of binary aqueous mixtures of organic solvents with partial miscibility is studied, with the interface seen as a region where phase segregation begins prior to bulk segregation (i.e., prior to liquid–liquid equilibrium). The phenomenon, called “surface segregation”, is a step toward understanding liquid segregation at a molecular level.

Binary liquid mixtures with partial miscibility segregate into two liquid phases when their overall composition lies within an interval defined by the two saturated phases. Out of this interval, there is one single phase, either solvent-rich or solute-rich. For most systems, in the solvent-rich phase, surface tension of the liquid–air interface decreases steeply with increasing solute concentration. This decrease is due to solute adsorption; hence, solute concentration at the surface is larger than in the bulk, leading to the hypothesis that phase

segregation starts at the surface, at bulk concentrations below the saturation point. When studying the foam stability of organic solvents mixtures with partial miscibility, Nishioka et al.⁷ described adsorption as “a precursor to phase separation, with the surface offering a region for partial segregation of molecules prior to their more complete separation as a bulk phase”.⁷ Nishioka et al. only referred to the enrichment process of the surface with solute, as other authors also have.^{8–11} In the present work, the coexistence of two saturated surface phases lying in the liquid–air interfacial plane was investigated. This phenomenon of surface segregation was theoretically predicted through a thermodynamic stability test, experimentally observed by means of Brewster's angle microscopy, and further interpreted with the aid of molecular dynamics simulations, all pointing out to the confirmation of surface–surface equilibrium.

Traditionally, the energy minimization principle is used to determine whether a liquid mixture is stable in one single phase or it segregates into two liquid phases. Geometrically, the stability test relies on the convexity of the Gibbs energy as a function of the overall composition of the system.¹² If the surface of a liquid is regarded as an additional thermodynamic phase, its stability can be analyzed under the same principle. The test has been applied before to the surface of water insoluble surfactant mixtures that form Langmuir monolayers, finding partially miscible monolayers with phase separation at

Received: April 9, 2015

Revised: June 10, 2015

Published: July 19, 2015



ACS Publications

© 2015 American Chemical Society

10304

DOI: 10.1021/acs.jpcb.5b03450
J. Phys. Chem. B 2015, 119, 10304–10315

the liquid–air interface.^{13–15} In this work, the stability test was implemented for Gibbs surfaces of miscible or partially miscible systems, with bulk concentrations below the saturation points, to determine the coexistence of two surfaces in equilibrium.

The stability test requires surface composition. For insoluble surfactants, overall two-dimensional concentrations are directly calculated from the area in which surfactants are confined to.¹³ On the other hand, the surface composition of a Gibbs surface cannot be measured or calculated directly because components are distributed between the bulk and the surface. In a previous paper, a thermodynamic procedure for determining the absolute surface composition from surface tension and density data was reported.¹⁶ It is based on the clear differentiation between Gibbs solute excess and Guggenheim's excess, the former defined in terms of the Gibbs dividing surface, and the latter obeying a dividing surface that provides equal volumes for the bulk and the surface layer.¹⁷ The procedure provides the absolute two-dimensional surface concentrations of both solute and solvent in a finite-depth surface layer (not necessarily a monolayer). Thermodynamic consistency of the results can be corroborated through the same fundamental equations it was calculated from, independently of the nonthermodynamic surface thickness.

The surface stability test was applied to the binary systems, water–methanol and water–ethanol, and to the binary systems with partially miscibility, water–methyl acetate, water–ethyl acetate, water–propyl acetate, and water–butyl acetate, for which surface tension and density data were available. The infinite water solubility of methanol and ethanol in the surface is predicted in the same way it is predicted in the bulk. On the contrary, the surface stability test shows that the liquid–air interface of the alkyl acetates systems is constituted by two surface phases: a water-rich surface and an acetate-rich surface, even at bulk concentrations out of the liquid–liquid interval, showing that phase segregation begins at the surface before liquid–liquid equilibrium.

Theoretical predictions were confirmed through Brewster's angle microscopy. Images show acetate-rich domains at the liquid–air interface that evidence surface segregation. Observations were complemented with molecular dynamics simulations that show the diffusion of acetate molecules from the bulk toward the interface, where acetates assemble into clusters leading to a nonhomogeneous surface constituted by water-rich and acetate-rich regions, in accordance with the hypothesis of surface segregation prior to liquid–liquid equilibrium.

2. THEORY

2.1. Thermodynamic Surface Stability Test. Minimization of Gibbs energy at constant temperature and pressure establishes that a liquid binary system is stable in one single phase if eq 1 is satisfied.^{12,18}

$$\left(\frac{\partial^2 g}{\partial x_i^2} \right)_{T,p} > 0 \quad (1)$$

where g is the molar Gibbs energy of the mixture and x_i is the overall molar fraction of component i . Gibbs energy can be written as a function of the Gibbs energy of mixing Δg^M defined by eq 2.¹²

$$\Delta g^M \equiv g - \sum_i x_i g_i^0 \quad (2)$$

where g_i^0 is the molar Gibbs energy of pure component i at the same temperature and pressure of the mixture. Thus, the thermodynamic stability condition can be written in terms of Δg^M eq 3:

$$\left(\frac{\partial^2 \Delta g^M}{\partial x_i^2} \right)_{T,p} > 0 \quad (3)$$

Geometrically, eq 3 means that a liquid binary mixture is stable in one single phase if Δg^M is a concave-up function of x_i ; otherwise, the system segregates into two saturated phases, whose compositions, x_{sat} and x'_{sat} , respectively, are given by the points with a common tangent line as illustrated in Figure 1.^{12,18} Molar fractions x_{sat} and x'_{sat} define the liquid–liquid

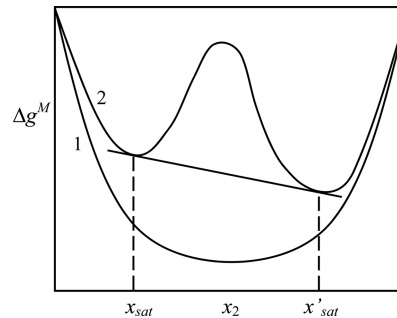


Figure 1. Gibbs energy of mixing of binary systems solvent (1) – solute (2) as a function of solute molar fraction; curve 1 belongs to a miscible system, and curve 2 belongs to a partially miscible system. The tangent line defines the liquid–liquid interval $x_{\text{sat}} < x_2 < x'_{\text{sat}}$.

equilibrium interval. Below x_{sat} and above x'_{sat} the system is stable in one single phase, either solvent-rich or solute-rich.

Eq 3 does not take into account adsorption, and therefore, it does not predict the existence of an interface. Thus, eq 3 is not useful to predict surface segregation. Instead, if the surface is regarded as a thermodynamic phase, the Gibbs energy of a surface g^s of constant area \mathcal{A} is given by Euler's eq eq 4,

$$g^s = \sum_i x_i^s \mu_i \text{ constant } T, p, \text{ and } \mathcal{A} \quad (4)$$

where x_i^s is the molar fraction of component i at the surface and μ_i is its chemical potential. In the same way as for a bulk phase, the Gibbs energy of a surface $\Delta g^{M,s}$ is defined by eq 5.

$$\Delta g^{M,s} \equiv g^s - \sum_i x_i^s g_i^0 \quad (5)$$

Therefore, a stable surface must satisfy the Gibbs energy minimization principle given by eq 6.

$$\left(\frac{\partial^2 \Delta g^{M,s}}{\partial x_i^2} \right)_{T,p} > 0 \quad (6)$$

If the surface is in equilibrium with the liquid bulk, chemical potentials in both phases are the same^{19,20} and are given by eq 7,¹²

$$\mu_i - \mu_i^0 = RT \ln x_i + RT \ln \gamma_i \quad (7)$$

where $\mu_i^0 = g_i^0$, and γ_i is the activity coefficient of component i . Eqs 4, 5, and 7 yield the final expression for $\Delta g^{M,s}$:

$$\Delta g^{M,s} = RT \sum_i x_i^s \ln x_i + RT \sum_i x_i^s \ln \gamma_i \quad (8)$$

Eq 8 is analogous to the Gibbs energy of mixing of a liquid bulk phase, eq 9,¹²

$$\Delta g^M = RT \sum_i x_i \ln x_i + RT \sum_i x_i \ln \gamma_i \quad (9)$$

the only difference being that $\Delta g^{M,s}$ depends additionally on the surface composition. For a binary mixture, the convexity of the curve $\Delta g^{M,s}$ vs x_i^s will determine if a single-phase surface satisfies the stability criterion of eq 6 or if the surface must segregate into two phases.

2.2. Surface Composition. A thermodynamic procedure for the calculation of the total (absolute) composition of a finite-depth surface was reported in a previous paper.¹⁶ It is based on the concepts of Gibbs solute excess (obeying Gibbs dividing surface) and Guggenheim's excess (obeying a dividing surface that provides equal volumes for the bulk and for the surface). An overview of the equations is provided in this section.

For a binary system solvent (1) – solute (2), Gibbs solute excess $\Gamma_2^{(1)}$ is given by the Gibbs adsorption equation, eq 10,²¹

$$\Gamma_2^{(1)} = -\frac{1}{RT} \left(\frac{d\sigma}{d \ln a_2} \right)_T \quad (10)$$

where σ is the surface tension of the mixture and a_2 is the solute activity. A binary mixture of unitary area contains N_1 moles of solvent and $(N_2 + \Gamma_2^{(1)})$ moles of solute. Adopting a calculation base of 1 mol of solvent, the volume V of a system with a liquid–air interface is given by eq 11

$$V = \bar{v}_1 + \left(\frac{x_2}{x_1} + \Gamma_2^{(1)} \right) \bar{v}_2 \quad (11)$$

where \bar{v}_1 and \bar{v}_2 are the partial molar volumes of component 1 and 2, respectively. The volume of a liquid bulk, without interface, is given by eq 12,

$$V = N_1 \bar{v}_1 + N_2 \bar{v}_2 \quad (12)$$

which divided by N_2 affords the amount of solute N_2^b contained in a liquid bulk with the same volume V of the system with the liquid–air interface, eq 11:

$$N_2^b = \frac{V}{\left(\frac{x_1}{x_2} \bar{v}_1 + \bar{v}_2 \right)} \quad (13)$$

N_2 in eq 13 has been distinguished with the superscript “*b*” to emphasize that it is the amount of solute in a bulk phase. The amount of solvent is obtained by means of eq 14.

$$N_1^b = \left(\frac{x_1}{x_2} \right) N_2^b \quad (14)$$

The difference between the amount of solute in the system with the liquid–air interface ($x_2/x_1 + \Gamma_2^{(1)}$) and in the bulk phase N_2^b yields the solute excess concentration Γ_2^{exc} , eq 15.

$$\Gamma_2^{\text{exc}} = \left(\frac{x_2}{x_1} + \Gamma_2^{(1)} \right) - N_2^b \quad (15)$$

The solvent excess is given by eq 16.

$$\Gamma_1^{\text{exc}} = 1 - N_1^b \quad (16)$$

The two-dimensional volumetric concentration Γ_i^{vol} is the amount of component i per unit area contained in a volume with the same thickness d of the surface, eq 17.

$$\Gamma_i^{\text{vol}} = \frac{x_i}{v} d \quad (17)$$

where (x_i/v) is i 's bulk molar concentration. The surface thickness d is estimated from the partial molar volume of the component with the larger volume, regarding the molecules as spheres of diameter, d , eq 18.

$$d = \left(\frac{6 \bar{v}_2}{\pi N_{Av}} \right)^{1/3} \text{ for } \bar{v}_2 > \bar{v}_1 \quad (18)$$

where N_{Av} is Avogadro's number.

The total two-dimensional concentrations in the finite-depth surface layers, Γ_1 and Γ_2 , are given by eq 19,

$$\Gamma_i = \Gamma_i^{\text{exc}} + \Gamma_i^{\text{vol}} \quad (19)$$

Surface molar fractions can be directly computed from Γ_i :

$$x_i^s = \frac{\Gamma_i}{\Gamma_1 + \Gamma_2} \quad (20)$$

Thermodynamic consistency of the results can be corroborated through the same fundamental equations it was calculated from, independently of the nonthermodynamic surface thickness.¹⁶

3. EXPERIMENTAL AND SIMULATION METHODS

3.1. Sample Preparation and Surface Tension Measurements. Acetates were purchased from Sigma-Aldrich with ReagentPlus purity (methyl acetate, 99%; ethyl acetate, ≥ 99.7%; propyl acetate, ≥ 99.5%; butyl acetate ≥ 99.5%). Solvents were used as received without further purification. Water was double distilled and degasified.

Surface tension of water-rich solutions was reported in a previous paper.²² In this work, surface tension of the acetate-rich solutions and of the aqueous and organic saturated phases was measured with the pending drop volume method with a TTV2 (Lauda) tensiometer (the same method was used for the water-rich solutions). Details of the instrumentation have been described previously.²³ To prevent acetate evaporation during the drop formation, 3 to 5 mL of the sample was poured in the cell in which drops are collected to obtain a saturated atmosphere. Temperature was controlled with a HAAKE NK22 water bath and monitored with a thermometer, Traceable; fluctuations were smaller than ±0.03 K. Surface tension data is provided in Table S.1 of the Supporting Information. Uncertainty is estimated to be ±0.05 mN/m.

Binary mixtures were prepared by mass using a SHIMADZU balance with precision of 10^{-4} g. The saturated phases were obtained by adding an excess of acetate to the water until having two liquid phases. The mixture was constantly stirred in a separation funnel and kept in a water bath at 298.15 K. The aqueous phase was extracted, and the organic phase remained in the funnel.

3.2. Brewster's Angle Microscopy. The liquid–air interface of the binary water-rich solutions was analyzed with a Brewster's angle microscope MicroBAM 3 (KSV Instruments LTD), with a HeNe laser with wavelength of 659 nm, set in a fixed angle of 53° with respect to the interface normal. The field of view is 3.6 × 4.0 mm, with a resolution of 6 μm/pixel. The

sample cell was a Langmuir trough of 50 mL (KSV Instruments LTD), with channels for thermostatic fluid (water). Both the microscope and the trough were placed on an antivibration table Halcyonics i4 (Accurion).

Before every observation, the liquid–air interface of pure water was checked free of any material, and surface tension was tested to be area-independent. Surface pressure is measured with a rod-shaped sensor, lifted by capillary forces when it is brought into contact with the liquid. The sensor must be placed in an area between the mobile barriers of the Langmuir trough. If the surface of pure water is free of impurities, the surface pressure should be zero and it must be independent of the area of the surface, varied by displacing the trough barriers.

Temperature of the Langmuir trough was set on 298.15 K. However, since the trough is an open cell, temperature was estimated to vary ± 1 K. To avoid liquid–liquid segregation in the water–acetate mixtures, acetates concentration was lower enough than the bulk saturation concentration x_{sat} to warrant the observation of a one-liquid-phase system. Binary mixtures were mechanically stirred and then sonicated in a Branson 1510 equipment. Sonication was necessary to ensure the solubilization of acetates in water. Samples were analyzed after different sonication periods, and after a different number of days they were prepared to avoid nonequilibrium conditions. Once poured in the Langmuir trough, solutions were analyzed for up to 90 min. In this time, lateral movement of acetate-rich domains due to Brownian movement was detected, with domains coming in and out of the field of view. In some cases, the trough barriers were slid to analyze a different area of the surface, with no significant changes in the images as expected for Gibbs surfaces, whose constitution is independent of the area of the surface. Observations reported in this work were triple checked.

The bulk solutions were analyzed by means of Dynamic Light Scattering (DLS). Analyses were performed with a NICOMP 380 ZLS (Particle Size Systems), which did not show the presence of an organic phase in the aqueous phase: no particles or acetate clusters with diameters larger than 1 nm were detected, which warrants the solubilization of acetates. Solubilization will be further discussed in Section 4.2.

3.3. Simulation Method. Molecular dynamics simulations of the bulk and the liquid–air interface of the system water–ethyl acetate were carried out using the GROMACS software, version 4.5.4.²⁴ Ethyl acetate was chosen because its water solubility is higher than the solubility of propyl acetate and butyl acetate. This allows simulating systems with a higher number of acetate molecules for a given size of the simulation box. Methyl acetate was discarded because, commonly, the properties of the shortest member of a family deviate from the members with larger alkyl chains.²⁵

Simulations were performed under the 53A6 force field.²⁶ United-atom coordinates and force field parameters of ethyl acetate were taken from the Automated Topology Builder (ATB) repository.²⁷ Bond lengths were constrained using the LINCS algorithm.²⁸ Water was simulated with the standard SPC/E model,²⁹ with bonds constrained with the SETTLE algorithm.³⁰ The van der Waals interactions were cut off at 1.2 nm. Long-range electrostatic interactions were treated with the particle-mesh Ewald summation method.³¹ Simulations were carried out in the NPT and NVT ensembles, with $T = 298.15$ K and $p = 1$ bar. Temperature was kept constant using the velocity rescaling algorithm.³² Pressure was kept constant through an isotropic coupling using the Parrinello–Rahman

algorithm.³³ The compressibility of ethyl acetate was $\kappa_T = 1.08 \times 10^{-4}$ 1/bar.³⁴ Periodic boundary conditions were applied in all directions. Newton equations were solved with the leapfrog integrator,³⁵ with a time step of 2 fs.

Simulation of 1000 molecules of ethyl acetate in the NPT ensemble for 10 ns provided a liquid density of $\rho = 0.9216$ g/cm³ (average over the last 5 ns), close to the experimental density $\rho_{\text{exp}} = 0.895$ g/cm³.³⁶ The use of long-range dispersion corrections leads to higher densities, so no corrections were applied. The simulated vaporization enthalpy was $\Delta h_{\text{vap}} = 37.68$ kJ/mol, also close to the experimental value of $\Delta h_{\text{vap,exp}} = 35.6$ kJ/mol.³⁷ The liquid–air (vacuum) interface was simulated in the NVT ensemble, using the liquid configuration obtained in the NPT ensemble. Two simulation boxes were built, one with a liquid phase of $5 \times 5 \times 4$ nm³ with 535 acetate molecules and another of $8 \times 8 \times 6$ nm³ with 2151 acetate molecules. Liquid interfaces were obtained by three-folding the Z axis. The correction for the evaluation of electrostatic interactions in the Z direction was introduced to produce a pseudo2d summation.²⁴ Surface tension was independent of the thickness of the liquid phase (Z direction). The average surface tension over the last 5 ns was $\sigma = 24.97$ mN/m, also matching the experimental value of $\sigma_{\text{exp}} = 23.93$ mN/m.

Simulation of the liquid–air (vacuum) interface of water provided a surface tension $\sigma = 51.15$ mN/m. Similar values have been reported using the SPC/E model.³⁸ Results are independent of the size of the simulation box as well. Two box sizes were tried, one with 1585 water molecules and the other with 3342. The difficulty on reproducing the surface tension of pure water is well-known and surface tensions between 50 and 60 mN/m are accepted.³⁸ The use of more sophisticated water models for reproducing the experimental surface tension $\sigma_{\text{exp}} = 71.81$ mN/m³⁶ is out of the scope of this work.

Simulations of water–ethyl acetate mixtures were performed with an acetate molar fraction $x_2 = 0.01$. At this concentration, surface segregation is predicted through the thermodynamic stability test. The bulk was simulated from a grid of acetate molecules solvated with water, in the NPT ensemble. Three simulation boxes were tested, with 48, 100, and 216 acetate molecules. The sizes of the boxes are reported in Table S.8 of the Supporting Information. The two smaller systems were simulated for 10 ns and the larger system for 25 ns. The average density over the last 5 ns is $\rho = 0.9694$ g/cm³, which agrees fairly well with the experimental density $\rho_{\text{exp}} = 0.99672$ g/cm³.³⁹ Results are independent of the size of the system.

Liquid–air interfaces were simulated in the NVT ensemble from different starting configurations; two starting configurations with $x_2 = 0.01$, with 48 and 100 acetate molecules, and one with $x_2 = 0.02$, with 216 acetate molecules. Details of the simulation boxes are given in Table S.9 of the Supporting Information. The starting configuration of the system with 48 molecules is the final configuration of the previous simulation of the bulk. The other two were the solvated grids. Simulations were carried out for 10 and 20 ns. The average surface tension over the last 5 ns is $\sigma = 49.6$ mN/m, which agrees fairly well with the experimental $\sigma_{\text{exp}} = 42.57$ mN/m. Results are independent of the size of the system. Final configurations will be discussed in Section 4.3.

4. RESULTS AND DISCUSSION

4.1. Surface Composition and Thermodynamic Surface Stability.

The surface stability of aqueous binary mixtures is determined by the convexity of the curve $\Delta g^{M,s}$ vs x_i^s .

According to eq 6, if the curve is concave-up, the surface is stable in one single phase; otherwise, the surface segregates into two phases. The Gibbs energy of mixing of the surface is given by eq 8, and the surface molar fractions are calculated with eqs 10 to 20.

Surface molar fractions of methanol and ethanol in aqueous binary mixtures were calculated in a previous work.¹⁶ Results match the experimental surface composition reported by Raina et al.^{40,41} and with the empiric mixing rule of Laaksonen for the surface tension of a binary mixture, eq 21.⁴² Salonen et al.⁴³ agreed that the Laaksonen rule fairly reproduces the experimental data of Raina et al.

$$\sigma = \frac{x_1^s \bar{v}_1 \sigma_1 + x_2^s \bar{v}_2 \sigma_2}{x_1^s \bar{v}_1 + x_2^s \bar{v}_2} \quad (21)$$

For both systems water (1) – alcohol (2), the van Laar model proves to best describe the activity coefficients.^{44–46} Parameters are provided in Section S.2 of the Supporting Information. The stability diagrams $\Delta g^{M,s}$ vs x_2^s at 298.15 K are shown in Figure 2. As expected for infinitely soluble systems,

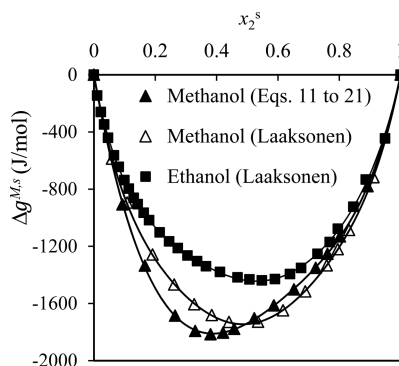


Figure 2. Gibbs energy of mixing of the surface as a function of alcohol surface molar fraction at 298.15 K. The source of the surface molar fractions is in parentheses.

the stability curves are concave-up in the entire concentration range $0 < x_2^s < 1$, independent of the source of surface molar fractions (Laaksonen rule or eqs 10 to 20), indicating that the surface of the binary aqueous mixtures of methanol and ethanol is stable in one homogeneous phase, just as the liquid bulk.

For the partially miscible systems water (1) – acetate (2), surface composition was calculated from surface tension using eqs 10 to 20. To obtain Gibbs acetate excess $\Gamma_2^{(1)}$, activity a_2 was calculated using van Laar activity coefficients. Parameters were taken from the literature^{47–49} and are reported in Table S.2 of the Supporting Information. With these coefficients, the van Laar model is able to predict the liquid–liquid composition interval $x_{\text{sat}} < x_2 < x'_{\text{sat}}$ as described in Figure 1, with Δg^M given by eq 9. The acetate molar fraction in the aqueous saturated phase is x_{sat} and in the organic phase is x'_{sat} . Results are reported in Table 1. Three-suffix Margules model was also tested, but it afforded smaller fractions x_{sat} than van Laar.

Gibbs acetate excess $\Gamma_2^{(1)}$ was determined from the slope of the curve σ vs $\ln a_2$, eq 10. In the water-rich region (aqueous region, $0 < x_2 < x_{\text{sat}}$), data was fitted to a second-degree polynomial, and in the acetate-rich region (organic region, $x'_{\text{sat}} < x_2 < 1$), data was fitted to a straight line. In the organic region, the slope is practically zero since surface tension depends scarcely on concentration.

Table 1. Acetates Molar Fractions in the Aqueous Saturated Phase x_{sat} and in the Organic Saturated Phase x'_{sat} at 298.15 K

	x_{sat}		x'_{sat}	
	van Laar	lit.	van Laar	lit.
methyl acetate	0.0561	0.0684 ^a 0.0731 ^b	0.8052	0.6970 ^a
ethyl acetate	0.0156	0.0158 ^c 0.0163 ^d 0.0176 ^b	0.9096	0.8267 ^d 0.8658 ^c
propyl acetate	0.0043	0.0038 ^c 0.0045 ^b	0.8708	0.9091 ^c
butyl acetate	0.0009	0.0009 ^c 0.00093 ^b 0.0010 ^d	0.8932	0.9323 ^c 0.9356 ^d

^aRef 50, $T = 313.24$ K, and $p = 53.1$ kPa. ^bRef 36. ^cRef 51, from interpolation at 298.15 K. ^dRef 52.

The partial molar volumes needed in eqs 11, 13, and 18 were obtained from the density data of Sakurai et al.³⁹ For methyl acetate, Iglesias et al.²⁵ provided densities in a wider composition range, with values matching Sakurai et al. data in the dilute region. No densities of acetate-rich solutions were found, except for methyl acetate.²⁵ For the rest of the acetates, density in this region was calculated as the sum of the densities of pure compounds weighted by their molar fractions. Since the acetates molar fractions in the organic region approach one, density is practically equal to the density of pure acetates. In all cases, the molar volume v of the binary mixtures depends linearly on the acetate molar fraction x_2 , both in the aqueous and in the organic region (an example is shown in Figure S.1 of the Supporting Information); thereby, the partial molar volumes of water and acetates are constant within the intervals $0 < x_2 < x_{\text{sat}}$ and $x'_{\text{sat}} < x_2 < 1$. Partial molar volumes are listed in Table S.3 of the Supporting Information.

For the calculation of the two-dimensional concentrations Γ_i^{vol} , eq 17, the minimum feasible surface thickness d_{\min} is that which provides a unitary surface molar fraction for the aqueous saturated phase (i.e., when $x_2 = x_{\text{sat}}$, $x_2^s = 1$). It is unlikely that the surface of the aqueous saturated phases is constituted by pure acetates ($x_2^s = 1$) because at this point the surface tension of the mixtures is higher than the surface tension of the pure acetates (see Table S.1 of the Supporting Information). For the systems of ethyl, propyl, and butyl acetates, eq 18 provides a surface thickness $d > d_{\min}$ (see Table S.4 of Supporting Information), leading to reasonable surface molar fractions in the entire concentration interval. However, for methyl acetate, eq 18 provides $d < d_{\min}$, yielding surface molar fractions larger than one. Thus, for methyl acetate, a surface thickness of $1.15d$ was used. Impact of surface thickness on the prediction of surface segregation will be analyzed below.

Two-dimensional concentrations Γ_i^{exc} (eqs 15 and 16), Γ_i^{vol} (eq 17), and Γ_i (eq 19) are reported in Table S.1 of the Supporting Information. Their meaning and behavior were discussed in ref 16. Thermodynamic consistency of the results can be consulted in Section S.5. Surface molar fractions x_2^s eq 20 are also reported in Table S.1 of the Supporting Information. Figure 3 shows that the acetates concentration in the surface is higher than in the bulk (i.e., $x_2^s > x_2$), as expected for surface active species. Surface molar fractions are consistent with the length of the alkyl chain of the acetates; the longer the alkyl chain, the higher the hydrophobicity and thus

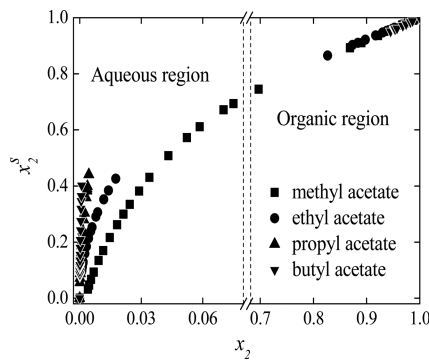


Figure 3. Surface molar fraction x_2^s vs bulk molar fraction x_2 at 298.15 K. Note the discontinuity in the abscise axis.

the adsorption. Hence, for a given bulk concentration, butyl acetate shows the highest surface concentration, followed by propyl acetate, ethyl acetate, and finally methyl acetate.

Surface stability diagrams $\Delta g_{M,s}^{M,s}$ vs x_2^s are shown in Figure 4, with $\Delta g_{M,s}^{M,s}$ given by eq 8. The aqueous and the organic regions are separated by the bulk immiscibility gap $x_2^s(x_{\text{sat}}) < x_2^s < x_2^s(x'_{\text{sat}})$ (dashed vertical lines). It is not possible to build the diagram throughout the entire composition range because the surface molar fractions are not available within the immiscibility gap; calculation of surface molar fractions requires surface tension data as a function of bulk composition, which is not available within the interval $x_{\text{sat}} < x_2 < x'_{\text{sat}}$. The Gibbs energy of mixing $\Delta g_{M,s}^{M,s}$ is a concave-up function of x_2^s in each the aqueous and the organic regions, satisfying the surface stability condition given by eq 6. However, in the aqueous region, there is an outright minimum. This means that if the stability diagram could be built in the entire composition range, $\Delta g_{M,s}^{M,s}$ would

necessarily display a concave-down behavior within the immiscibility gap, signifying that the surface of the water-acetate mixtures is not stable in one single phase, but it segregates into two phases with compositions x_{sat}^s and x'_{sat}^s , respectively, defined by the points with a common tangent line as shown in Figure 4, where it is seen that the bulk immiscibility gap lies within the surface immiscibility gap. Surface molar fractions of the saturated surfaces, x_{sat}^s and x'_{sat}^s , and the corresponding bulk molar fractions $x_2(x_{\text{sat}}^s)$ and $x_2(x'_{\text{sat}}^s)$ are reported in Table 2. In the aqueous region, the bulk concentration at which surface segregation is predicted $x_2(x_{\text{sat}}^s)$ is smaller than the bulk concentration of the aqueous saturated phase x_{sat} , reported in Table 1. For example, for methyl acetate, $x_2(x_{\text{sat}}^s) = 0.0225 < x_{\text{sat}} = 0.0731$. In the organic region, the bulk concentration at which surface segregation is predicted $x_2(x'_{\text{sat}}^s)$ lies above the bulk molar fraction of the organic saturated phase x'_{sat} . For methyl acetate: $x_2(x'_{\text{sat}}^s) = 0.8709 > x'_{\text{sat}} = 0.6970$. In summary: $x_2(x_{\text{sat}}^s) < x_{\text{sat}} < x_2 < x'_{\text{sat}} < x_2(x'_{\text{sat}}^s)$. This means that phase segregation starts at the surface, at bulk concentrations below the saturation point (left to $x_2^s(x_{\text{sat}})$) and right to $x_2^s(x'_{\text{sat}})$ in Figure 4). Once bulk saturation compositions are reached, liquid–liquid equilibrium is observed. In other words, surface segregation precedes bulk segregation.

Water solubility of acetates x_{sat} decreases periodically upon the increase of the alkyl chain. The same periodicity is kept in the bulk molar fractions at which surface segregation is predicted $x_2(x_{\text{sat}}^s)$, as shown in Figure 5. As mentioned before, $x_2(x_{\text{sat}}^s) < x_{\text{sat}}$; however, $x_{\text{sat}}^s > x_{\text{sat}}$, showing that in the surface it is possible to attain higher solute concentrations. The surface molar fractions x_{sat}^s do not follow the same periodicity as x_{sat} . In comparison with the decrease of x_{sat} , it could be said that x_{sat}^s

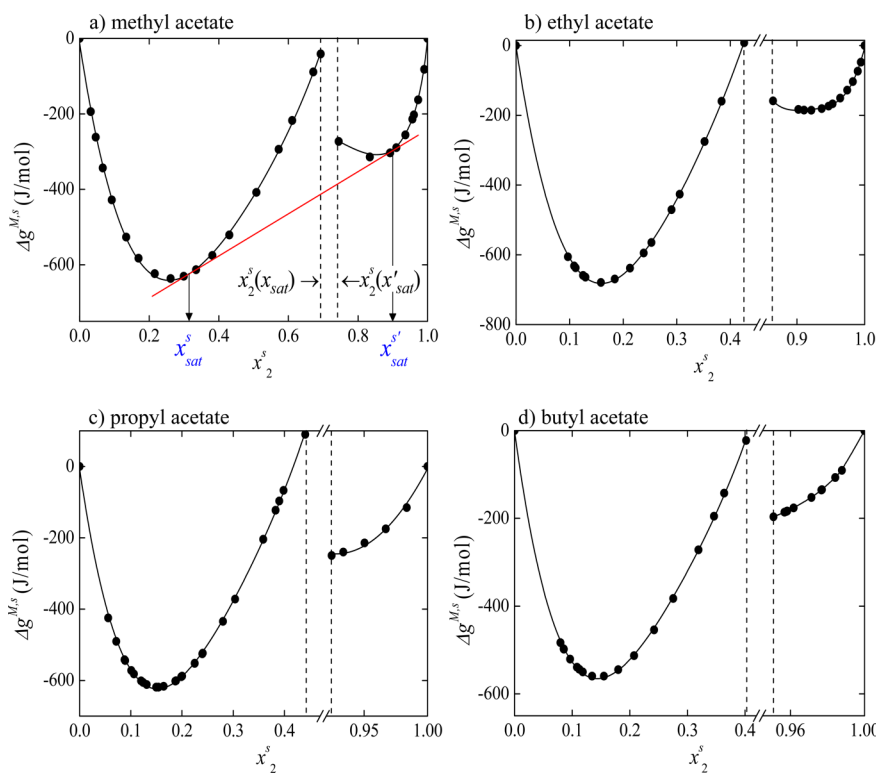


Figure 4. Gibbs energy of mixing of the surface as a function of acetate surface molar fraction at 298.15 K. Dashed vertical lines indicate the bulk immiscibility gap $x_2^s(x_{\text{sat}}) < x_2^s < x_2^s(x'_{\text{sat}})$.

Table 2. Surface Molar Fractions in the Saturated Surfaces x_{sat}^s and $x_{\text{sat}}^{s'}$, and the Corresponding Bulk Molar Fractions $x_2(x_{\text{sat}}^s)$ and $x_2(x_{\text{sat}}^{s'})$ at 298.15 K

	aqueous region		organic region		
	surface thickness d	x_{sat}^s ^a	$x_2(x_{\text{sat}}^s)$ ^b	$x_{\text{sat}}^{s'}$ ^a	$x_2(x_{\text{sat}}^{s'})$ ^b
methyl acetate ^c	0.3119	0.0225	0.8943	0.8709	
ethyl acetate	0.1798	0.0032	0.9457	0.9288	
propyl acetate	0.1670	0.0009	0.9334	0.9198	
butyl acetate	0.1439 ^d	0.00019			
surface thickness $1.15d$					
	x_{sat}^s ^a	$x_2(x_{\text{sat}}^s)$ ^b	$x_{\text{sat}}^{s'}$ ^a	$x_2(x_{\text{sat}}^{s'})$ ^b	
methyl acetate ^e	0.2372	0.0210	0.8936	0.8736	
ethyl acetate	0.1360	0.0028	0.9407	0.9247	
propyl acetate	0.1196	0.0007	0.9306	0.9182	
butyl acetate	0.1049 ^d	0.00017			

^aDetermined numerically by fitting two-degree or fourth-degree polynomials to the plots Δg^{M_s} vs x_2^s . At x_{sat}^s and $x_{\text{sat}}^{s'}$, the tangent line has the same slope and the same intercept. ^bDetermined numerically from the plot x_2^s vs x_2 . ^c $d = 1.15d_{\min}$. ^dDetermined from the minimum of the plot Δg^{M_s} vs x_2^s . ^e $1.15d = 1.15(1.15d_{\min})$.

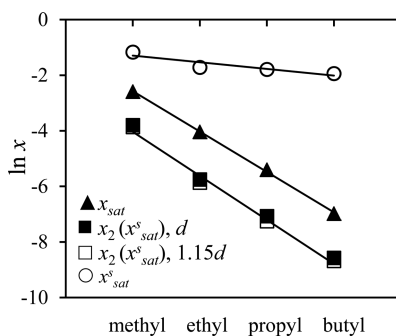


Figure 5. Bulk and surface molar fractions in the organic region, for surface thicknesses d and $1.15d$, as a function of the number of alkyl carbon atoms in the acetates.

are almost constant throughout the four systems (see also Table 2), pointing out to a common orientation of the acetates at the liquid–air interface, with the alkyl chain toward the air in order to project a common area on the surface.

In the organic region, no clear periodicity in the bulk molar fractions x'_{sat} and $x_2(x'_{\text{sat}})$ is noticed (see Figure 6). The surface molar fractions $x_{\text{sat}}^{s'}$ do not show an outright trend either. It can only be said that $x_{\text{sat}}^{s'} > x'_{\text{sat}}$ due to adsorption, as

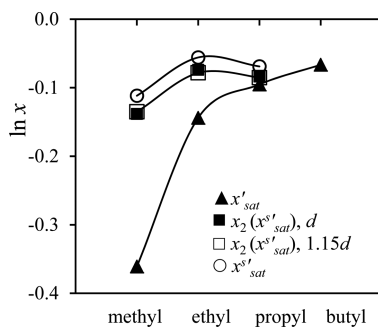


Figure 6. Bulk and surface molar fractions in the organic region, for surface thicknesses d and $1.15d$, as a function of the number of alkyl carbon atoms in the acetates.

in the aqueous region. These results are ascribed to the difficulty of measuring surface tensions in the organic region, where dependence on bulk composition is practically null.

The larger the surface thickness d , the smaller the surface molar fractions x_2^s are.¹⁶ Surface thickness was augmented 15% with respect to thickness d given by eq 18, representing an average increase of 1 Å, which is of the order of van der Waals radius and covalent bonds.⁵³ In the aqueous region, this increment makes the surface molar fractions x_{sat}^s decrease around 25% (see Table 2). However, the corresponding bulk molar fractions $x_2(x_{\text{sat}}^s)$ only decrease between 5% and 10%, as shown in Figure 5, without modifying surface segregation predictions, and without making the previous discussion lose any generality. In the organic region, surface thickness impact on both $x_{\text{sat}}^{s'}$ and $x_2(x_{\text{sat}}^{s'})$ is less than 1%.

4.2. Brewster's Angle Microscopy (BAM) Images.

Brewster's angle images show that the surface of the aqueous binary mixtures of acetates is constituted by an aqueous and an organic phase, the latter in the form of acetate-rich domains. For methyl acetate, the number of acetate-rich domains increases with bulk concentration, as shown in Figure 7 and

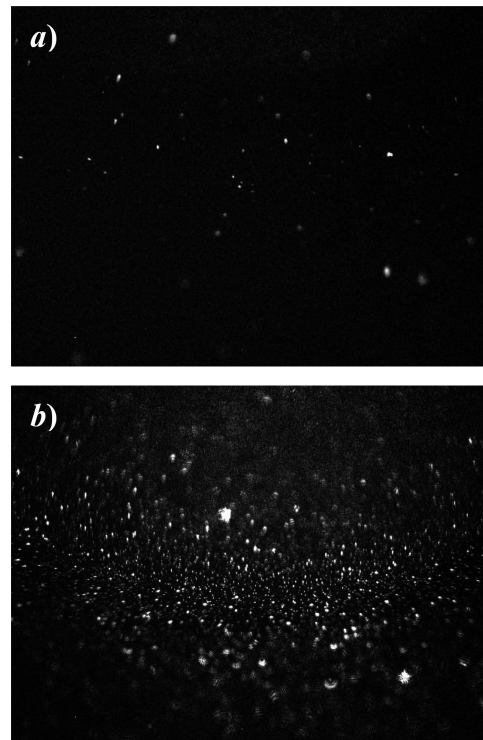


Figure 7. BAM images of water–methyl acetate mixtures with $x_2 > x_2(x_{\text{sat}}^s)$: (a) $x_2 = 0.0350$ and (b) $x_2 = 0.0595$. Note that the focus of these images is located in the center. Far from focus, domains are enlarged and blurred.

Figure S.3 of the Supporting Information. Bulk concentrations in Figure 7 are larger than the bulk concentration $x_2(x_{\text{sat}}^s)$ at which surface saturation is predicted ($0.0210 < x_2(x_{\text{sat}}^s) < 0.0225$, see Table 2). At lower concentrations, no acetate-rich domains were detected, although in some cases, isolated and very diffuse domains appeared, which probably indicates that the surface thickness is larger than $1.15d_{\min}$ such that the fraction $x_2(x_{\text{sat}}^s)$ is actually smaller. Images for systems with $x_2 < x_2(x_{\text{sat}}^s)$ are provided in Section S.6.1 of the Supporting Information.

For propyl acetate and butyl acetate, acetate-rich domains were detected at bulk concentrations $x_2 > x_2(x_{\text{sat}}^s)$ as well. However, due to their lower water solubility, the increment of domains with bulk concentration is not as evident as for methyl acetate. Figure 8 and Figure 9 show images for both systems,



Figure 8. BAM image of water–propyl acetate, $x_2 = 0.002 > x_2(x_{\text{sat}}^s)$.



Figure 9. BAM image of water–butyl acetate, $x_2 = 0.0007 > x_2(x_{\text{sat}}^s)$.

respectively. More images are provided in Sections S.6.2 and S.6.3 of the Supporting Information. At lower concentrations, $x_2 < x_2(x_{\text{sat}}^s)$, no domains were detected.

For ethyl acetate, no domains were detected at any concentration. These results are ascribed to the high volatility of ethyl acetate since the sample cell is an open Langmuir trough. Indeed, methyl acetate is more volatile; however, its larger solubility allows attaining higher concentrations at which acetate-rich domains are detected.

During preliminary tests for butyl acetate, the difficulty of solubilizing acetates in water was noticed. The liquid–air interface of a sample which was stirred manually was replete with acetate, as shown in Figure 10. DLS experiments did not show an organic liquid phase or any acetate clusters in the bulk larger than 1 nm. These results indicate that although the acetate molecules that are incorporated into the bulk form an aqueous solution, manual stirring is not enough to ensure complete bulk solubilization before the acetate adsorbs in the surface (i.e., adsorption prevails over solubilization). To ensure solubilization, samples were sonicated for 30 min. BAM images in Section S.6.3 of the Supporting Information show that sonication for 30 min is equivalent to 12 h of mechanical stirring. Furthermore, BAM observations are independent of the age of the samples, which range from 1 to 8 days after they were sonicated. In this period, hydrolysis effects are discarded since according to Handorf and Washburn,⁵⁴ an aqueous solution of 2 M methyl acetate hydrolyses 0.74% in 6 days and

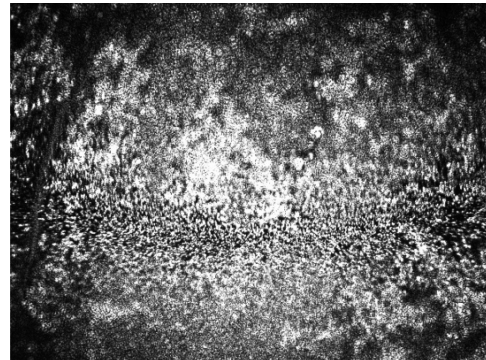


Figure 10. BAM image of water–butyl acetate, $x_2 = 0.0007 > x_2(x_{\text{sat}}^s)$, manual stirring.

7.95% in 18 days. Sonication, age-independent observations, and no hydrolysis point out that solutions were analyzed under equilibrium conditions, with all possible acetate molecules solubilized in water.

For DLS experiments, water was filtered through a 200 nm filter. Samples were analyzed 20, 60, and 120 min and 1 day after they were prepared. In all cases, no particles larger than 1 nm were detected in the bulk, so the acetate-rich domains observed in Figures 7 to 9, with diameters between 10 and 20 μm , are formed in the surface due to surface interactions and not due to bulk interactions. In the acetates systems, the organic phase is lighter than the aqueous phase. Therefore, it is fair to ask whether the acetate-rich domains are a true surface phase or if it is a bulk organic phase lying over the aqueous one. To avoid any doubts, BAM and DLS experiments were performed on an aqueous solution of chloroform with $x_2 = 0.0009$. Chloroform density is larger than water density, so a bulk organic phase would lie at the bottom of the trough, and it would not be detected by BAM. However, chloroform-rich domains were observed as shown in Figure 11, and DLS did not show any aggregates or clusters in the bulk. Thus, organic domains in BAM images are true surface phases, outgrowth of surface interactions.



Figure 11. BAM image of water–chloroform, $x_2 = 0.0012$.

Chloroform is twice volatile than ethyl acetate at 298.15 K.³⁶ Though, the infinite dilution activity coefficient of chloroform in water is 10 times larger than the activity coefficient of ethyl acetate ($\gamma_{\text{CHCl}_3}^\infty = 800–1000 \gg \gamma_{\text{AcEtO}}^\infty = 73.9$),⁴⁸ so the higher hydrophobicity of chloroform makes the formation of organic domains easier.

4.3. Molecular Dynamics Simulations. Before simulating the liquid–air interface of the system water–ethyl acetate, the liquid bulk was simulated. In the three simulations performed in the *NPT* ensemble, the starting configurations were the solvated grids with an acetate molar fraction $x_2 = 0.01$ (with 48, 100, and 216 acetate molecules). In all final configurations, acetate molecules were not scattered throughout the bulk, but they aggregated into clusters as shown in Figure 12. Similar

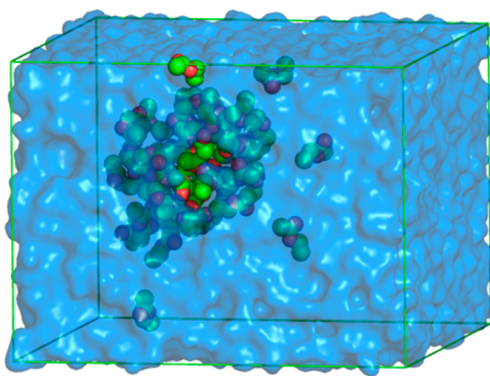


Figure 12. Snapshot at 10 ns of the liquid bulk of the system water–ethyl acetate, with $x_2 = 0.01$, at 298.15 K and 1 bar.

results were reported by Gupta and Patey⁵⁵ for the aqueous system of 2-butoxyethanol at 300 K and 1 bar, under simulation parameters very close to this work, except for the pressure coupling algorithm (Berendsen instead of Parrinello-Rahman). Despite the infinite water solubility of 2-butoxyethanol, 2-butoxyethanol aggregates were obtained, independently of the water model (SPC/E or TIP3P) and the force field (S3A6 or CHARMM27), either united-atom or all-atom. Gupta and Patey contrasted their results with the formation of pseudomicelles⁵⁶ in which water molecules are trapped within the 2-butoxyethanol aggregates. However, Gupta and Patey simulated systems with 32000 molecules (water plus 2-butoxyethanol) for 10 ns. This time seems short for such a large system. Probably, if simulations had run longer, clusters of pure 2-butoxyethanol would have been observed, without trapped water molecules inside, as in the case of ethyl acetate.

In an additional simulation for a larger system with 729 acetate molecules and 69609 water molecules, four initial aggregates merged into two and finally into one, along 50 ns. These results show the difficulty of solubilizing acetates in water, even at acetate concentrations below saturation ($x_2 = 0.01 < x_{\text{sat}} = 0.0176$), as was noticed in the BAM experiments. However, these final configurations of clusters, with no dispersed solution phase, do not match the DLS experiments showing no aggregates in the bulk larger than 1 nm (all clusters in simulations are larger than 1 nm); either, clusters are smaller or a dispersed solution phase is expected. Therefore, the analysis of simulations will remain qualitative, focusing on diffusion of acetates from the bulk to the surface.

Simulations of the liquid–air interface were performed in the *NVT* ensemble from different starting configurations of the liquid phase. Two simulations were run with $x_2 = 0.01$, one with 48 acetate molecules and the other with 100. At this concentration, surface segregation is predicted ($x_2 = 0.01 > x_2(x_{\text{sat}}^*) = 0.0032$). The starting configuration of the system with 48 molecules was the configuration of the bulk shown in Figure 12. In the presence of an interface, the cluster dissociates itself as the acetate molecules migrate toward the interface (Figure 13a), matching with the experimental observations that point out that adsorption prevails over solubilization. As the acetate molecules arrive to the surface, instead of clustering, they first extend along the interface (Figure 13b), and then they aggregate again to show an interface with two regions: a water-rich phase and an acetate-rich phase (Figure 13c). The dissociation of the cluster and the posterior aggregation of the acetates at the interface support that the acetate-rich domains observed in the BAM images are formed in the surface and are not the result of bulk clustering.

The starting configuration of the simulation with 100 acetate molecules was the grid of $5 \times 5 \times 4$ acetates. The thin depth of the liquid phase in the Z direction (5.86 nm) hinders the formation of a cluster in the bulk. Instead, the acetate molecules migrate directly toward the liquid–air interface, where they aggregate into an acetate-rich domain. In a third simulation with $x_2 = 0.02$, with 216 acetate molecules, the liquid phase is thick enough (6.99 nm) to allow the molecules farther from the interface form clusters in the bulk (Figure 14a); however, these

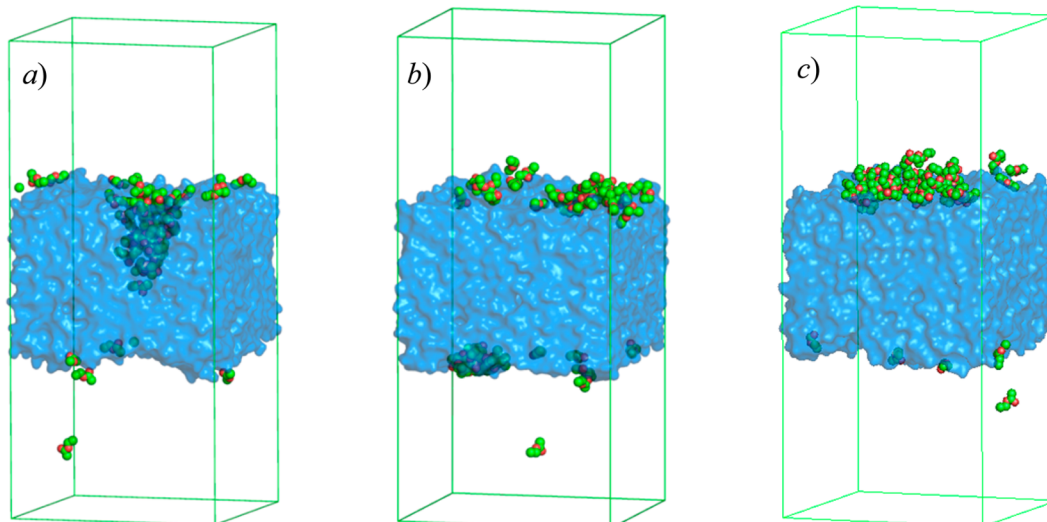


Figure 13. Snapshots of the system water–ethyl acetate at 298.15 K, with $x_2 = 0.01$, with 48 acetate molecules, (a) 0.7 ns, (b) 1 ns, and (c) 10 ns.

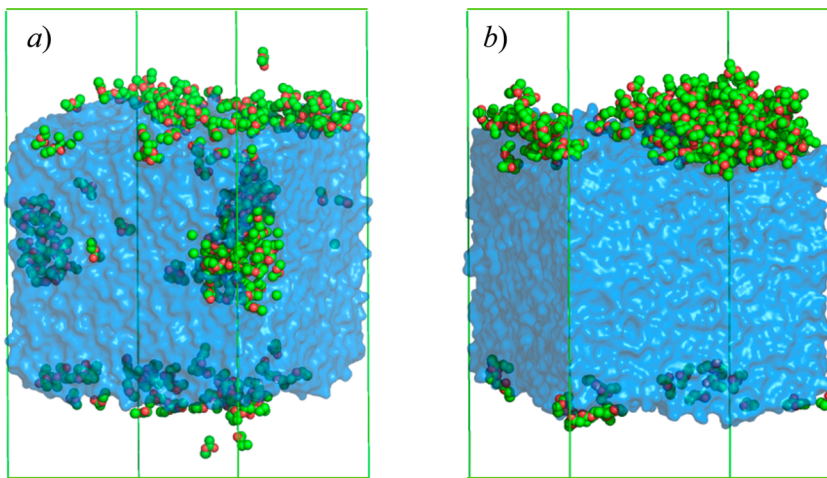


Figure 14. Snapshots of the system water–ethyl acetate at 298.15, with $x_2 = 0.02$, with 216 acetate molecules, (a) 2 and (b) 20 ns. Only part of the air (vacuum) phase is shown.

clusters dissociate themselves as they migrate to the interface, in the same way as in the simulation with 48 molecules, for finally aggregating again in the surface (Figure 14b). Note that even if the area of the more concentrated system (49 nm^2) is smaller than the area of the system with 100 molecules with half of the concentration (53.7 nm^2), the surface is still not fully covered of acetate molecules, but they form acetate-rich-domains.

CONCLUSIONS

The liquid–air interface of the aqueous binary mixtures with partial miscibility of methyl acetate, ethyl acetate, propyl acetate, and butyl acetate is constituted by an aqueous and an organic saturated surface. The thermodynamic stability test shows that the surface of these systems is unstable in one single phase; in order to minimize its energy, the surface must segregate into two saturated phases: a water-rich surface and an acetate-rich surface. The surface immiscibility gap contains the bulk immiscibility gap [$x_2(x_{\text{sat}}^s) < x_{\text{sat}} < x_2 < x'_{\text{sat}} < x_2(x'_{\text{sat}})$], showing that surface segregation is predicted at bulk concentrations below the saturation points (i.e., surface segregation is predicted before liquid–liquid equilibrium).

In the saturated surfaces, the acetates concentration is higher than in the saturated liquids ($x_{\text{sat}}^s > x_{\text{sat}}$), indicating that there is more room for the acetates at the surface than in the bulk, in good agreement with the adsorption process. The composition of the saturated water-rich surface (x_{sat}^s) is practically constant for the four systems studied, pointing out to a common orientation of the short alkyl chain acetates at the liquid–air interface. On the other hand, the bulk molar fractions at which surface segregation is predicted [$x_2(x_{\text{sat}}^s)$] keep the decreasing periodicity of the water solubility of the acetates, from methyl to butyl acetate, showing the consistency of the relationship between bulk and surface molar fractions.

Brewster's angle microscopy confirmed the theoretical predictions of surface segregation. Images show acetate-rich domains at the liquid–air interface. These domains are the result of surface interactions, as it was proved by the DLS analysis of the bulk, which did not show any aggregates of the size of the domains detected at the surface. Observations on the aqueous system of chloroform support this conclusion; due to the higher density of an organic liquid phase, no domains at the liquid–air interface would have been detected. Still, organic

domains were observed, in the same way as in the interface of the alkyl acetates solutions.

Sample preparation under different stirring conditions revealed the difficulty of solubilizing the alkyl acetates in water and showed that adsorption prevails over solubilization, which further supports the findings of phase segregation starting at the liquid–air interface. Interpretation of experiments agree with the molecular dynamics simulations, which show the diffusion of acetate molecules from the bulk toward the interface, where acetate molecules aggregate into acetate-rich domains. Even when in the bulk there were acetate clusters, these aggregates dissociated themselves as they migrated to the interface, where molecules extended along the surface, for finally aggregating again. This behavior indicates that acetate-rich domains are formed at the surface as the result of surface interactions and not due to bulk clustering.

ASSOCIATED CONTENT

Supporting Information

Surface tension, two-dimensional surface concentrations, van Laar parameters, partial molar volumes, surface thickness, the thermodynamic consistency test of the absolute surface composition, Brewster's angle microscopy images, and details of the simulation boxes. The Supporting Information is available free of charge on the ACS Publications website at DOI: [10.1021/acs.jpcb.Sb03450](https://doi.org/10.1021/acs.jpcb.Sb03450).

AUTHOR INFORMATION

Corresponding Author

*Address: Ave. Universidad 3000, México, D. F., 04510, México. E-mail: jgraciaf@unam.mx. Tel: +52 55 56223899, ext. 44462. Fax: +52 55 56162010.

Notes

The authors declare no competing financial interest.

ACKNOWLEDGMENTS

The authors thank Dr. Ángel Piñeiro from Universidad de Santiago de Compostela for his advice in the molecular dynamics simulations and Dr. José Campos-Terán for giving us access to the BAM microscope of UAM-Cuajimalpa and for his instruction in its use. C. B.-S. is grateful to Consejo Nacional de Ciencia y Tecnología for Grant 223384 for Ph.D. studies. Dirección General de Asuntos del Personal Académico

(DGAPA) is also acknowledged for financial support (PAPIIT-IN114015).

■ REFERENCES

- (1) Cabral, J. T.; Hudson, S. D. Microfluidic approach for rapid multicomponent interfacial tensiometry. *Lab Chip* **2006**, *6*, 427–436.
- (2) Nishiyama, K.; Jinno, N.; Hashimoto, M.; Tsukagoshi, K. Mixing process of ternary solvents prepared through microchannels in a microchip under laminar flow conditions. *Anal. Sci.* **2012**, *28*, 423–427.
- (3) Halim, U.; Zheng, C. R.; Chen, Y.; Lin, Z.; Jiang, S.; Cheng, R.; Huang, Y.; Duan, X. A rational design of cosolvent exfoliation of layered materials by directly probing liquid-solid interaction. *Nat. Commun.* **2013**, *4*, 2213–2219.
- (4) Coleman, J. N.; Lotya, M.; O'Neill, A.; Bergin, S. D.; King, P. J.; Khan, U.; Young, K.; Gaucher, A.; De, S.; Smith, R. J.; et al. Two-dimensional nanosheets produced by liquid exfoliation of layered materials. *Science* **2011**, *331*, 568–571.
- (5) Hernández-Pascacio, J.; Garza, C.; Banquy, X.; Díaz-Vergara, N.; Amigo, A.; Ramos, S.; Castillo, R.; Costas, M.; Piñeiro, Á. Cyclodextrin-based self-assembled nanotubes at the water/air interface. *J. Phys. Chem. B* **2007**, *111*, 12625–12630.
- (6) Born, P.; Schön, V.; Blum, S.; Gerstner, D.; Huber, P.; Kraus, T. Self-assembly of gold nanoparticles at the oil-vapor interface: from mono- to multilayers. *Langmuir* **2014**, *30*, 13176–13181.
- (7) Nishioka, G. M.; Lacy, L. L.; Facemire, B. R. The Gibbs surface excess in binary miscibility gap systems. *J. Colloid Interface Sci.* **1981**, *80*, 197–207.
- (8) Utigard, T.; Toguri, J. M. Surface segregation and surface tension of liquid mixtures. *Metall. Trans. B* **1987**, *18*, 695–702.
- (9) McLure, I. A.; Soares, V. A. M.; Williamson, A.-M. Total surface segregation: A fresh look at the Gibbs adsorption isotherm for binary liquid mixtures. *Langmuir* **1993**, *9*, 2190–2201.
- (10) Novakovic, R.; Giuranno, D.; Ricci, E.; Tuissi, A.; Wunderlich, R.; Fecht, H.-J.; Egry, I. Surface, dynamic and structural properties of liquid Al-Ti alloys. *Appl. Surf. Sci.* **2012**, *258*, 3269–3275.
- (11) Koirala, I.; Singh, B. P.; Jha, I. S. Theoretical assessment on segregating nature of liquid In-Tl alloys. *J. Non-Cryst. Solids* **2014**, *398–399*, 26–31.
- (12) Walas, S. M. *Phase Equilibria in Chemical Engineering*; Butterworth Publishers: Stoneham, 1985.
- (13) Lee, Y.-L.; Lin, J.-Y.; Chang, C.-H. Thermodynamic characteristics and Langmuir Blodgett deposition behavior of mixed DPPA/DPPC monolayers at air/liquid interfaces. *J. Colloid Interface Sci.* **2006**, *296*, 647–654.
- (14) Hao, C.; Sun, R.; Zhang, J. Mixed monolayers of DOPC and palmitic acid at the liquid-air interface. *Colloids Surf., B* **2013**, *112*, 441–445.
- (15) He, G.; Sun, R.; Hao, D.; Yang, J.; Wang, M.; Zhang, L. Thermodynamic analysis and AFM study of the interaction of palmitic acid with DPPE in Langmuir monolayers. *Colloids Surf., A* **2014**, *441*, 184–194.
- (16) Bermúdez-Salguero, C.; Gracia-Fadrique, J. Gibbs excess and the calculation of the absolute surface composition of liquid binary mixtures. *J. Phys. Chem. B* **2015**, *119*, 5598.
- (17) Guggenheim, E. A.; Adam, N. K. The thermodynamics of adsorption at the surface of solutions. *Proc. R. Soc. London, Ser. A* **1933**, *139*, 218–236.
- (18) Prausnitz, J. M.; Lichtenthaler, R. M.; Gomes de Azevedo, E. *Termodinámica Molecular de los Equilibrios de Fases*, 3rd ed.; Prentice Hall: Madrid, 2000.
- (19) Fawcett, W. R. *Liquids, Solutions and Interfaces: From Classical Macroscopic Descriptions to Modern Microscopic Details*; Oxford University Press: New York, 2004.
- (20) Bermúdez-Salguero, C.; Gracia-Fadrique, J. Surface chemical potential from a surface equation of state vs. Butler's equation. *Fluid Phase Equilib.* **2014**, *375*, 367–372.
- (21) Adamson, A. *Physical Chemistry of Surfaces*, 3rd ed.; John Wiley & Sons: New York, 1976.
- (22) Bermúdez-Salguero, C.; Gracia-Fadrique, J.; Amigo, A. Surface tension data of aqueous binary mixtures of methyl, ethyl, propyl and butyl acetates at 298.15 K. *J. Chem. Eng. Data* **2010**, *55*, 2905–2908.
- (23) Piñeiro, Á.; Brocos, P.; Amigo, A.; Pintos, M.; Bravo, R. Surface tension and refractive indices of (tetrahydrofuran + *n*-alkanes) at *T* = 298.15 K. *J. Chem. Thermodyn.* **1999**, *31*, 931–942.
- (24) van der Spoel, D.; Lindahl, E.; Hess, B.; van Buuren, A. R.; Apostol, E.; Meulenhoff, P. J.; Tieleman, D. P.; Sijbers, A. L. T. M.; Feenstra, K. A.; van Drunen, R.; Berendsen, H. J. C. *Gromacs User Manual versión 4.5.4*; www.gromacs.org, 2010.
- (25) Iglesias, M.; Marino, G.; Orge, B.; Piñeiro, M. M.; Tojo, J. Liquid-liquid equilibria, and thermodynamic properties of the system methyl acetate + methanol + water at 298.15 K. *Phys. Chem. Liq.* **1999**, *37*, 193–213.
- (26) Oostenbrink, C.; Villa, A.; Mark, A. E.; van Gunsteren, W. F. A biomolecular force field based on the free enthalpy of hydration and solvation: The GROMOS force field parameter sets 53A5 and 53A6. *J. Comput. Chem.* **2004**, *25*, 1656–1676.
- (27) Malde, A. K.; Zuo, L.; Breeze, M.; Stroet, M.; Poger, D.; Nair, P. C.; Oostenbrink, C.; Mark, A. E. An automated force field topology builder (ATB) and repository: version 1.0. *J. Chem. Theory Comput.* **2011**, *7*, 4026–4037.
- (28) Hess, B.; Bekker, H.; Berendsen, H. J. C.; Fraaije, J. G. E. M. LINCS: A linear constraint solver for molecular simulations. *J. Comput. Chem.* **1997**, *18*, 1463–1472.
- (29) Berendsen, H. J. C.; van der Spoel, D.; van Drunen, R. GROMACS: A message passing parallel molecular dynamics implementation. *Comput. Phys. Commun.* **1995**, *91*, 43–56.
- (30) Miyamoto, S.; Kollman, P. A. SETTLE: An analytical version of the SHAKE and RATTLE algorithms for rigid water models. *J. Comput. Chem.* **1992**, *13*, 952–962.
- (31) Darden, T.; York, D.; Pedersen, L. Particle mesh Ewald: An Nln(N) method for Ewald sums in large systems. *J. Chem. Phys.* **1993**, *98*, 10089–10092.
- (32) Bussi, G.; Donadio, D.; Parrinello, M. Canonical sampling through velocity rescaling. *J. Chem. Phys.* **2007**, *126*, 014101.
- (33) Parrinello, M.; Rahman, A. Polymorphic transitions in single crystals: A new molecular dynamics method. *J. Appl. Phys.* **1981**, *52*, 7182–7190.
- (34) Gardas, R. L.; Johnson, I.; Vaz, D. M. D.; Fonseca, I. M. A.; Ferreira, A. G. M. PVT property measurements for some aliphatic esters from (298 to 393) K and up to 35 MPa. *J. Chem. Eng. Data* **2007**, *52*, 737–751.
- (35) Hockney, R. W.; Goel, S. P.; Eastwood, J. Quiet high resolution computer models of a plasma. *J. Comput. Phys.* **1974**, *14*, 148–158.
- (36) Riddick, J.; Bunger, W.; Sakano, T. *Organic Solvents, Physical Properties and Methods of Purification*, 4th ed.; John Wiley & Sons: New York, 1986.
- (37) Nilsson, S.-O.; Wadsö, I. Thermodynamic properties of some mono-, di-, and tri-esters enthalpies of solution in water at 288.15 to 318.15 K and enthalpies of vaporization and heat capacities at 298.15 K. *J. Chem. Thermodyn.* **1986**, *18*, 673–681.
- (38) Wang, J.; Zeng, X. C. Computer simulation of liquid-vapor interfacial tension: Lennard-Jones fluid and water revisited. *J. Theor. Comput. Chem.* **2009**, *08*, 733–763.
- (39) Sakurai, M.; Nakamura, K.; Nitta, K. Partial molar volumes of alkyl acetates in water. *J. Chem. Eng. Data* **1996**, *41*, 1171–1175.
- (40) Raina, G.; Kulkarni, G. U.; Rao, C. N. R. Mass spectrometric determination of the surface composition of ethanol-water mixtures. *Int. J. Mass Spectrom.* **2001**, *212*, 267–271.
- (41) Raina, G.; Kulkarni, G. U.; Rao, C. N. R. Surface enrichment in alcohol-water mixtures. *J. Phys. Chem. A* **2001**, *105*, 10204–10207.
- (42) Laaksonen, A. Nucleation of binary water –*n*-alcohol vapors. *J. Chem. Phys.* **1992**, *97*, 1983–1989.
- (43) Salonen, M.; Malila, J.; Napari, I.; Laaksonen, A. Evaluation of surface composition of surface active water – alcohol type mixtures: A comparison of semiempirical models. *J. Phys. Chem. B* **2005**, *109*, 3472–3479.

- (44) Strey, R.; Viisanen, Y.; Aratono, M.; Kratochvil, J. P.; Yin, Q.; Friberg, S. E. On the necessity of using activities in the Gibbs equation. *J. Phys. Chem. B* **1999**, *103*, 9112–9116.
- (45) Yano, Y. F. Correlation between surface and bulk structures of alcohol-water mixtures. *J. Colloid Interface Sci.* **2005**, *284*, 255–259.
- (46) Gmehling, J.; Onken, U.; Rarey-Nies, J. R. *Vapor-Liquid Equilibrium Data Collection. Aqueous Systems*, Suppl. 2 (in Chemistry Data Series: Vol. 1, part 1b); DECHEMA: Frankfurt, 1988.
- (47) Kojima, K.; Zhang, S.; Hiaki, T. Measuring methods of infinite dilution activity coefficients and a database for systems including water. *Fluid Phase Equilib.* **1997**, *131*, 145–179.
- (48) Gmehling, J.; Menke, J.; Schiller, M. *Activity Coefficients at Infinite Dilution*; Vol. IX, part 4, DECHEMA: Frankfurt, 1994.
- (49) Viades-Trejo, J.; Gracia-Fadrique, J. A new surface equation of state. Hydrophobic-hydrophilic contributions to the activity coefficient. *Fluid Phase Equilib.* **2008**, *264*, 12–17.
- (50) Hsieh, C.-T.; Lee, M.-J.; Lin, H.-M. Vapor-liquid-liquid equilibria for aqueous systems with methyl acetate, methyl propionate, and methanol. *Ind. Eng. Chem. Res.* **2008**, *47*, 7927–7933.
- (51) Stephenson, R.; Stuart, J. Mutual binary solubilities: Water – alcohols and water – esters. *J. Chem. Eng. Data* **1986**, *31*, 56–70.
- (52) del Carmen Grande, M.; Marschhoff, C. M. Liquid-liquid equilibria for water + benzonitrile + ethyl acetate or butyl acetate. *J. Chem. Eng. Data* **2005**, *50*, 1324–1327.
- (53) Morrison, R. T.; Boyd, R. N. *Química Orgánica*, 3rd ed.; Fondo Educativo Interamericano: Boston, 1976.
- (54) Handorf, B. J.; Washburn, E. R. The change in the surface tension of a solution of methyl acetate due to hydrolysis. *J. Am. Chem. Soc.* **1935**, *57*, 1201–1203.
- (55) Gupta, R.; Patey, G. N. Association and microheterogeneity in aqueous 2-butoxyethanol solutions. *J. Phys. Chem. B* **2011**, *115*, 15323–15331.
- (56) Elizalde, F.; Gracia-Fadrique, J.; Costas, M. Effect of aggregates in bulk and surface properties. Surface tension, foam stability, and heat capacities for 2-butoxyethanol + water. *J. Phys. Chem.* **1988**, *92*, 3565–3568.